

# $U(1)_{B_3-L_2}$ Explanation of the Neutral Current $B$ -Anomalies

B. C. Allanach<sup>1</sup>

<sup>1</sup>DAMTP, University of Cambridge, Wilberforce Road, Cambridge, CB3 0WA, United Kingdom

Received: date / Accepted: date

**Abstract** We investigate a speculative short-distance force, proposed to explain discrepancies observed between measurements of certain neutral current decays of  $B$  hadrons and their Standard Model predictions. The force derives from a spontaneously broken, gauged  $U(1)_{B_3-L_2}$  extension to the Standard Model, where the extra quantum numbers of Standard Model fields are given by third family baryon number minus second family lepton number. The only fields beyond those of the Standard Model are: three right-handed neutrinos, a gauge field associated with  $U(1)_{B_3-L_2}$  and a Standard Model singlet complex scalar which breaks  $U(1)_{B_3-L_2}$ , a ‘flavon’. This simple model, via interactions involving a TeV scale force carrying  $Z'$  vector boson, can successfully explain the neutral current  $B$ -anomalies whilst accommodating other empirical constraints. A combination of up-to-date  $B$ -anomaly fits, LHC direct  $Z'$  search limits and  $B_s - \bar{B}_s$  mixing bounds imply that  $M_{Z'} > 1.9$  TeV at the 95% confidence level. The model possesses a *flavonstrahlung* signal, where  $pp$  collisions produce a  $Z'$  and a flavon, which subsequently decays into two Higgs bosons.

## 1 Introduction

Data from the first decade of running of Large Hadron Collider (LHC) experiments involving the decays of  $B$  hadrons show some discrepancies with Standard Model (SM) predictions. For example, measurements of the ratio of branching ratios  $R_{K^{(*)}} = BR(B \rightarrow K^{(*)}\mu^+\mu^-)/BR(B \rightarrow K^{(*)}e^+e^-)$  [1, 2],  $BR(B_s \rightarrow \mu^+\mu^-)$  [3, 4, 5, 6] and some angular distributions in  $K^*\mu^+\mu^-$  decays [7, 8, 9, 10, 11, 12] all show some discrepancy (there are others). Each

discrepant observable is only 1-4 $\sigma$  away from SM predictions but collectively, they point to a roughly similar conclusion. Despite a recent flagship LHCb measurement of  $R_K$  fluctuating somewhat toward its SM prediction (announced at the Moriond 2019 conference), the overall picture remains. Relative theoretical uncertainties, while taken into account in the number of sigma, vary from less than 1% to 20%, depending on the particular observable in question. In summary, several measurements of  $B$  hadron decays are somewhat inconsistent with the SM prediction of the  $(\bar{s}b)(\bar{\mu}\mu)$  effective coupling. We call these discrepancies the neutral current<sup>1</sup>  $B$ -anomalies (NCBAs).

Several different fits to over a hundred  $B$ -observables [14, 15, 16, 17, 18, 19] broadly agree: they favour a beyond the SM contribution to the weak effective theory operator

$$\mathcal{L}_{BSM} = -C_9 \mathcal{N} (\bar{s}\gamma^\rho P_L b) (\bar{\mu}\gamma_\rho \mu) + H.c., \quad (1)$$

where  $\mathcal{N} = 1/(36 \text{ TeV})^2$  (in the present paper,  $C_9 \neq 0$  means a contribution *beyond* the SM). We shall focus on one of the fits for definiteness: Ref. [17], where the result is that

$$C_9 = -0.97 \pm 0.15. \quad (2)$$

The coefficient of the operator at the best-fit point has a pull of 5.9 $\sigma$  away from the SM value of 0 (taking the operator with  $P_L$  inserted before the final  $\mu$  field in (1) provides an even better, but comparable, fit, 6.6 $\sigma$  away from the SM value).

One possibility to generate such beyond the SM contributions is from the interactions of a new electrically neutral, massive, force carrying particle, dubbed a  $Z'$ , which has family dependent interactions. In particular,

<sup>1</sup>This is to distinguish some other discrepancies in  $BR(B \rightarrow D^{(*)}\tau\nu)/BR(B \rightarrow D^{(*)}l\nu)$  [13], which are charged current processes and which we do not address here.

<sup>a</sup>e-mail: B.C.Allanach@damtp.cam.ac.uk

in order to explain the  $B$ -anomalies, the Lagrangian density should include (with the possible inclusion or exclusion of the second term) the interaction terms

$$\mathcal{L}_{int} = -g_{\mu_L} \overline{\mu_L} \not{Z}' \mu_L - g_{\mu_R} \overline{\mu_R} \not{Z}' \mu_R - g_{sb} \left( \overline{s_L} \not{Z}' b_L + H.c. \right), \quad (3)$$

where  $g_{sb}$ ,  $g_{\mu_L}$  and  $g_{\mu_R}$  are all dimensionless coupling constants. Once the  $Z'$  is integrated out, in the weak effective field theory, one obtains the Lagrangian density terms

$$\mathcal{L}_{WET} = -\frac{g_{sb} g_{\mu_L}}{M_{Z'}^2} (\overline{s_L} \gamma^\rho b_L) (\overline{\mu_L} \gamma_\rho \mu_L) - \frac{g_{sb} g_{\mu_R}}{M_{Z'}^2} (\overline{s_L} \gamma^\rho b_L) (\overline{\mu_R} \gamma_\rho \mu_R) + H.c. \quad (4)$$

These are precisely of the type that can explain the NCBA: identifying (1) and (4) we see that

$$C_9 = g_{sb} (g_{\mu_L} + g_{\mu_R}) (36 \text{ TeV} / M_{Z'})^2. \quad (5)$$

Many models of flavoured  $Z'$  vector bosons have been invented based on spontaneously broken gauged  $U(1)$  flavour symmetries [20, 21], for example from  $L_\mu - L_\tau$  and other groups [22, 23, 24, 25, 26, 27, 28, 29, 30, 31, 32, 33, 34, 35, 36, 37, 38, 39, 40, 41, 42, 43, 44, 45, 20, 46, 47, 48, 49, 50, 51, 52, 53, 54, 55, 56]. Some models have several abelian groups in the extension [57], while some others [58, 59] generate BSM contributions with loop-level penguin diagrams. Some of the models are more ambitious than others, providing more or less detail toward ultra-violet completion.

In Refs. [42, 44] a  $U(1)_{B_3-L_2}$  symmetry was proposed to explain the neutral current  $B$ -anomalies. Both papers are quite detailed in their exposition, providing information about fermion mass model building through additional vector-like representations of the gauge group. It is our purpose here to provide a simplified broad-brush formulation of the model and apply the latest bounds and fits, which have changed significantly since the model's conception.

The paper proceeds as follows: in §2, we define the model, examining the couplings to fermions, which are of paramount importance for phenomenology. To specify a model for phenomenological study, it is necessary to make further assumptions about quark mixing; these are made in §3. Then, in §4, we examine the consistency of NCBA fits with other experimental constraints. A novel signal process, *flavonstrahlung*, is identified. In §5, we provide a summary and discussion. Technical definitions of mixing matrices and fields are made available in Appendix A.

## 2 $B_3 - L_2$ Model

The gauge group of the model is  $SU(3) \times SU(2)_L \times U(1)_Y \times U(1)_{B_3-L_2}$ . We display the charge assignments

$Q'_{L_i}$	$u'_{R_i}$	$d'_{R_i}$	$L'_1$	$L'_2$	$L'_3$
0	0	0	0	-3	0
$e'_{R_1}$	$e'_{R_2}$	$e'_{R_3}$	$\nu'_{R_1}$	$\nu'_{R_2}$	$\nu'_{R_3}$
0	-3	0	0	-3	0
$Q'_{L_3}$	$u'_{R_3}$	$d'_{R_3}$	$H$	$\theta$	
1	1	1	0	$q_\theta$	

**Table 1**  $B_3 - L_2$  charge assignments of fields. A prime denotes a weak eigenstate Weyl fermion. Under  $SU(3) \times SU(2)_L \times U(1)_Y$ , the fields have representation  $Q'_{L_j} \sim (3, 2, 1/6)$ ,  $L'_{L_j} \sim (1, 2, -1/2)$ ,  $e'_{R_j} \sim (1, 1, -1)$ ,  $d'_{R_j} \sim (3, 1, -1/3)$ ,  $u'_{R_j} \sim (3, 1, 2/3)$ ,  $\nu'_{R_j} \sim (1, 1, 0)$ ,  $H = (H^+, H^0)^T \sim (1, 2, 1/2)$ , respectively.  $i \in \{1, 2\}$ ,  $j \in \{1, 2, 3\}$  are family indices. The flavon,  $\theta$ , is a SM-singlet complex scalar field and  $q_\theta$  is a non-zero rational real number.

of the fields in the model under  $U(1)_{B_3-L_2}$  in Table 1. The chiral fermions are all in *vector-like* representations with respect to  $U(1)_{B_3-L_2}$  and so standard arguments imply that the symmetry is free from local perturbative anomalies, given that the SM plus three right-handed neutrinos is free of gauge anomalies under  $SU(3) \times SU(2)_L \times U(1)_Y$ .

At the renormalisable unbroken level,  $U(1)_{B_3-L_2}$  predicts that the Yukawa matrices of SM fermions (see Appendix A for definitions and conventions) have the texture

$$Y_u \sim \begin{pmatrix} \times \times 0 \\ \times \times 0 \\ 0 0 \times \end{pmatrix}, Y_d \sim \begin{pmatrix} \times \times 0 \\ \times \times 0 \\ 0 0 \times \end{pmatrix}, Y_e \sim \begin{pmatrix} \times 0 \times \\ 0 \times 0 \\ \times 0 \times \end{pmatrix}, \quad (6)$$

where  $\times$  denotes an arbitrary dimensionless entry, which may be non-zero. From this prediction, we deduce that the Cabibbo-Kobayashi-Maskawa (CKM) matrix has zero entries for  $V_{ub}$ ,  $V_{cb}$ ,  $V_{ts}$  and  $V_{td}$ . However, the  $U(1)_{B_3-L_2}$  symmetry is spontaneously broken by the vacuum expectation value  $\langle \theta \rangle$  of a flavon: a SM singlet scalar  $\theta$  with non-zero  $B_3 - L_2$  charge  $q_\theta$ . This breaking will replace the zero entries in (6) by small corrections. The model then predicts that the magnitudes of the CKM matrix entries  $V_{ub}$ ,  $V_{cb}$ ,  $V_{ts}$  and  $V_{td}$  are suppressed from unity by some small factor. This qualitative prediction [42, 44] agrees with current experimental estimates:  $|V_{cb}| = (41.0 \pm 1.4) \times 10^{-3}$ ,  $|V_{ub}| = (3.82 \pm 0.24) \times 10^{-3}$ ,  $|V_{td}| = (8.0 \pm 0.3) \times 10^{-3}$ ,  $|V_{ts}| = (38.8 \pm 1.1) \times 10^{-3}$  [13]. We note that fermion mass data dictate that there should be hierarchies within the  $\times$  symbols of each matrix in (6). A more complete higher-scale theory could explain such hierarchies. The (33) entry of each matrix should *not* be suppressed, in order to explain the hierarchically large masses of third family fermions as compared to the other two families. Smaller corrections to the zeroes will then indeed pre-

dict small entries for the magnitudes of  $V_{ub}$ ,  $V_{cb}$ ,  $V_{ts}$  and  $V_{td}$ .

Neutrinos acquire mass through the see-saw mechanism with an initial symmetric mass matrix (whose basis is defined in (A.4)):

$$M_\nu = \begin{pmatrix} 0 & 0 & 0 & \dagger & 0 & \dagger \\ 0 & 0 & 0 & 0 & \dagger & 0 \\ 0 & 0 & 0 & \dagger & 0 & \dagger \\ \dagger & 0 & \dagger & * & 0 & * \\ 0 & \dagger & 0 & 0 & 0 & 0 \\ \dagger & 0 & \dagger & * & 0 & * \end{pmatrix}, \quad (7)$$

where the entries marked  $\dagger$  are of order the electroweak scale multiplied by the neutrino Yukawa couplings  $Y_\nu$  and we expect the entries marked  $*$  to be much greater than  $\dagger$ , since the mass scale  $*$  is not fixed to the electroweak scale by any symmetry. As it stands, (7) has two eigenvalues of order  $*$ , two of order  $\dagger$  and two of order  $\dagger^2/*$ . However, we expect some of the zeroes in (7) to be corrected by ‘small’ non-renormalisable corrections from the spontaneous breaking of  $U(1)_{B_3-L_2}$ : in particular, the bottom right-hand 3 by 3 sub-matrix will be corrected by terms of order  $*$  times a small number. It is expected that such corrections will still be many orders of magnitude above  $\dagger$ . Depending on the value of  $q_\theta$ , some of the other entries may be corrected by terms of order  $\langle\theta\rangle$ . However, it is not our intention here to go into the minutæ of fermion mass model building for the model; instead we shall be content with the ‘broad-brush’ sketch expected of three very light neutrinos and three very heavy ones resulting from the expected small corrections and the see-saw mechanism.

We begin with the couplings of the  $U(1)_{B_3-L_2}$  gauge boson  $Z'_\mu$  to fermions in the Lagrangian in the weak (primed) eigenbasis

$$\mathcal{L}_{Z'\psi} = -g_{Z'} \left( \overline{Q}'_{3L} \not{Z}' Q'_{3L} + \overline{u}'_{3R} \not{Z}' u'_{3R} + \overline{d}'_{3R} \not{Z}' d'_{3R} - 3\overline{L}'_{2L} \not{Z}' L'_{2L} - 3\overline{e}'_{2R} \not{Z}' e'_{2R} - 3\overline{\nu}'_{2R} \not{Z}' \nu'_{2R} \right), \quad (8)$$

where  $g'_{Z'}$  is the  $U(1)_{B_3-L_2}$  gauge coupling.  $U(1)_{B_3-L_2}$  is broken by  $\langle\theta\rangle \neq 0$  and so the  $Z'$  acquires a mass

$$M_{Z'} = q_\theta g_F \langle\theta\rangle. \quad (9)$$

We shall see below that a combination of LHC search bounds and NCBAAs will imply that  $M_{Z'}$  is at least of order the TeV scale. We assume that the approximately right-handed neutrinos discussed above have a much higher mass than  $M_{Z'}$ . The  $Z'$  boson ‘eats’ one real degree of freedom of  $\theta$  via the Brout-Englert-Higgs mechanism [60, 61] to form its longitudinal polarisation mode. We expand  $\theta = (\langle\theta\rangle + \vartheta)/\sqrt{2}$ , in terms of the one real physical flavon degree of freedom in the spontaneously broken theory,  $\vartheta$ . Its tree-level mass  $m_\vartheta$ , depends on

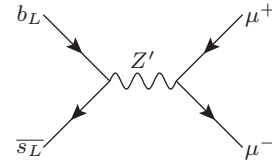


**Fig. 1** Tree-level Feynman diagram of a process which contributes to the NCBAAs.

free parameters in the  $\theta$  potential, but we expect it to be of order  $\langle\theta\rangle$ .

Writing the weak eigenbasis fermionic fields as 3-dimensional vectors in family space  $\mathbf{u}_{\mathbf{R}'}, \mathbf{Q}_{\mathbf{L}'} = (\mathbf{u}_{\mathbf{L}'}, \mathbf{d}_{\mathbf{L}'}), \mathbf{e}_{\mathbf{R}'}, \mathbf{d}_{\mathbf{R}'}, \mathbf{L}_{\mathbf{L}'} = (\nu_{\mathbf{L}'}, \mathbf{e}_{\mathbf{L}'})$ , we define the 3 by 3 unitary matrices  $V_P$ , where  $P \in \{u_R, d_L, u_L, e_R, u_R, d_R, \nu_L, e_L\}$ . These transform between the weak eigenbasis and the mass (unprimed) eigenbasis<sup>2</sup> as detailed in Appendix A:

$$\mathbf{P}' = V_P \mathbf{P}. \quad (10)$$

Re-writing (8) in the mass eigenbasis and using the quark and lepton mixing matrices  $V$  and  $U$  defined in (A.8)

$$\begin{aligned} \mathcal{L}_{Z'\psi} = & -g_{Z'} \left( \overline{\mathbf{d}}_{\mathbf{L}} \Lambda_{\Xi}^{(d_L)} \not{Z}' \mathbf{d}_{\mathbf{L}} + \overline{\mathbf{u}}_{\mathbf{L}} \Lambda_{\Xi}^{(u_L)} \not{Z}' \mathbf{u}_{\mathbf{L}} \right. \\ & + \overline{\mathbf{u}}_{\mathbf{R}} \Lambda_{\Xi}^{(u_R)} \not{Z}' \mathbf{u}_{\mathbf{R}} + \overline{\mathbf{d}}_{\mathbf{R}} \Lambda_{\Xi}^{(d_R)} \not{Z}' \mathbf{d}_{\mathbf{R}} \\ & - 3\overline{\mathbf{e}}_{\mathbf{L}} \Lambda_{\Omega}^{(e_L)} \not{Z}' \mathbf{e}_{\mathbf{L}} - 3\overline{\nu}_{\mathbf{L}} \Lambda_{\Omega}^{(\nu_L)} \not{Z}' \nu_{\mathbf{L}} \\ & \left. - 3\overline{\mathbf{e}}_{\mathbf{R}} \Lambda_{\Omega}^{(e_R)} \not{Z}' \mathbf{e}_{\mathbf{R}} - 3\overline{\nu}_{\mathbf{R}} \Lambda_{\Omega}^{(\nu_R)} \not{Z}' \nu_{\mathbf{R}} \right), \quad (11) \end{aligned}$$

we have defined the 3 by 3 dimensionless Hermitian coupling matrices

$$\Lambda_{\alpha}^{(I)} := V_I^{\dagger} \alpha V_I, \quad (12)$$

where  $I \in \{u_L, d_L, e_L, \nu_L, u_R, d_R, e_R, \nu_R\}$ ,  $\alpha \in \{\Xi, \Omega\}$  and

$$\Xi := \begin{pmatrix} 0 & 0 & 0 \\ 0 & 0 & 0 \\ 0 & 0 & 1 \end{pmatrix}, \quad \Omega := \begin{pmatrix} 0 & 0 & 0 \\ 0 & 1 & 0 \\ 0 & 0 & 0 \end{pmatrix}. \quad (13)$$

Provided that  $(V_{d_L})_{23} \neq 0$ , (11) contains tree-level couplings of the  $Z'$  to  $\overline{b}_L s_L$ ,  $\overline{s}_L b_L$  and  $\mu^+ \mu^-$ . Thus, it shows promise to explain the NCBAAs through processes such as the one in Fig. 1.

### 3 Example Case

In order to specify the model further, we should detail the mixing matrices  $V_I$ . However, we have not constructed a detailed model for them. Here, we shall make a simple ansatz for fermion mixing matrices which is likely to not be ruled out by other flavour bounds on

<sup>2</sup> $\mathbf{P}$  and  $\mathbf{P}'$  are column vectors.

flavour changing neutral currents but which is favourable from the point of view of the NCBAAs. For example, in order to successfully describe the NCBAAs, we require  $(V_{d_L})_{23} \neq 0$ . We shall examine the limit (which we call ‘ $(B_3 - L_2)\text{eg}$ ’) where

$$V_{d_L} = \begin{pmatrix} 1 & 0 & 0 \\ 0 & \cos \theta_{sb} & -\sin \theta_{sb} \\ 0 & \sin \theta_{sb} & \cos \theta_{sb} \end{pmatrix}, \quad (14)$$

$V_{d_R} = 1, V_{e_R} = 1, V_{e_L} = 1$  and  $V_{u_R} = 1$ , meaning that  $V_{u_L} = V_{d_L} V^\dagger, V_{\nu_L} = U^\dagger$ , where  $U$  is the lepton mixing matrix defined in Appendix A. Thus, the predicted tree-level flavour changing neutral currents are, aside from the  $Z'$  coupling to  $\bar{b}s$ , relegated to the up quarks and neutrinos, where the bounds from experiment are significantly weaker. Our assumptions here are of course strong, but they merely constitute an example case for early phenomenological study in order to assess viability. Extracting the couplings of the  $Z'$  relevant for the NCBAAs, we have

$$\mathcal{L} = -g_{Z'} \left[ \left( \frac{1}{2} \sin 2\theta_{sb} \bar{s} \not{Z}' P_L b + H.c. \right) - 3\bar{\mu} \not{Z}' \mu \right] + \dots (15)$$

Thus, by identifying (15) with (5), we have  $g_{sb} = (g_{Z'}/2) \sin 2\theta_{sb}$ ,  $g_{\mu_L} = g_{\mu_R} = -3g_{Z'}/2$ .

## 4 Phenomenology

We have now specified the  $(B_3 - L_2)\text{eg}$  enough to apply experimental constraints to it. We first bound its free parameters through the fit to the NCBAAs and then go on to derive other pertinent bounds before considering predictions.

### 4.1 Fit to NCBAAs

At energy scales far below  $M_{Z'}$ , in the effective theory where the  $Z'$  is integrated out, (15) becomes

$$\mathcal{L} = \frac{3g_{Z'}^2}{2M_{Z'}^2} \sin 2\theta_{sb} (\bar{s} \gamma^\rho P_L b) (\bar{\mu} \gamma_\rho \mu) + H.c., \quad (16)$$

where  $\gamma^\rho$  are Dirac matrices,  $P_L$  is a left-handed projection matrix and  $\rho \in \{0, 1, 2, 3\}$  is a space-time index. The fits prefer no sizeable contributions from the operator in (16) obtained by switching  $P_L \rightarrow P_R$  [17] and indeed, since we have assumed  $V_{d_R} = 1$ , we predict none (at tree level<sup>3</sup>). Substituting  $g_{sb}, g_{\mu_L}$  and  $g_{\mu_R}$  obtained above into (5), we have

$$\sin 2\theta_{sb} = -5.1 \times 10^{-4} \left( \frac{M_{Z'}}{g_{Z'} \text{TeV}} \right)^2 C_9. \quad (17)$$

<sup>3</sup>Our level of approximation is tree level throughout.

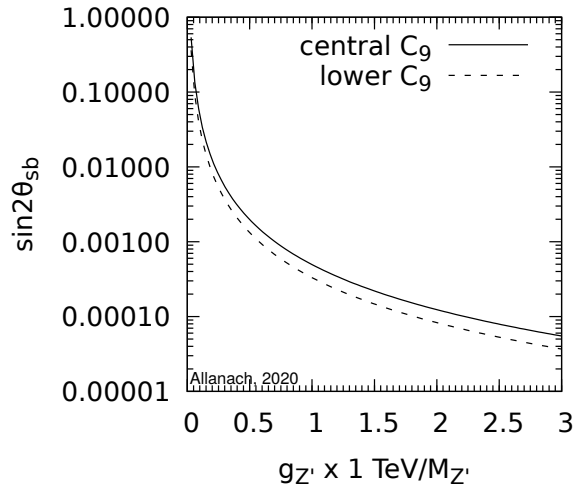


**Fig. 2**  $\sin 2\theta_{sb}$  in the  $(B_3 - L_2)\text{eg}$  as constrained by a fit [17] to the NCBAAs in (17). Central  $C_9 = -0.97$  and lower  $C_9 = -0.65$ .

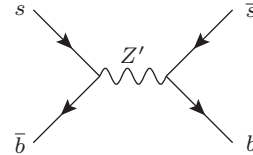


**Fig. 3** Tree-level Feynman diagram of a beyond the SM contribution to  $B_s - \bar{B}_s$  mixing.

Requiring that  $\sin 2\theta_{sb} \leq 1$  implies that

$$g_{Z'} \text{TeV}/M_{Z'} \geq 0.023 \sqrt{C_9/(-0.97)}. \quad (18)$$

The  $(B_3 - L_2)\text{eg}$  has three pertinent free parameters:  $M_{Z'}$ ,  $\theta_{sb}$  and  $g_{Z'}$ . It will suit us to adopt (17) with the inferred empirically-fitted input for  $C_9$  in order to reduce the number of free-parameters to two, so that the parameter space of the model can be captured and plotted in two dimensions. The central value of  $C_9$  as extracted from fits to the NCBAAs shown in (2) will be the ‘central  $C_9$ ’ value of -0.97, however we will also refer to the ‘lower  $C_9$ ’ value. This is the value of  $C_9$  which is closest to the SM limit but still fits the relevant data to within  $2\sigma$  (i.e.  $C_9 = -0.65$  [17]). We display the value of  $\sin 2\theta_{sb}$  for these two cases in Fig. 2.

### 4.2 $B_s - \bar{B}_s$ mixing

Since our  $Z'$  couples to bottom and strange quarks, it induces a beyond the SM contribution to  $B_s - \bar{B}_s$  mixing via the process in Fig. 3. The value of the bound depends on lattice data [62] which change the SM prediction. These have varied significantly over the last decade. We use a recent determination based on lattice

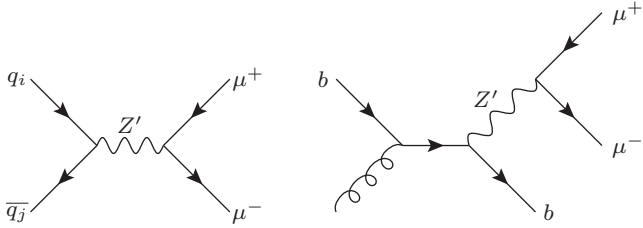


**Fig. 4** Example Feynman diagrams of tree-level  $B_3 - L_2$  inclusive  $Z'$  production at the LHC followed by decay into muons.  $q_{i,j} \in \{u, c, d, s, b\}$  are such that the combination  $q_i \bar{q}_j$  has zero electric charge.

data and sum rules [63] which implies that<sup>4</sup>  $g_{Z'} \sin 2\theta_{sb}/2 \leq M_{Z'}/194$  TeV [64]. Using (17), we obtain the lower bound

$$g_{Z'} \frac{\text{TeV}}{M_{Z'}} \geq 0.048 \frac{C_9}{-0.97}. \quad (19)$$

The fact that this is a *lower* bound might at first seem counter-intuitive, until one realises that, for lower values of  $g_{Z'} \text{TeV}/M_{Z'}$ , one can only fit the NCBA with a larger value of  $\sin 2\theta_{sb}$ , i.e. a larger  $Z'$  coupling to bottom and strange (anti-)quarks and therefore a larger contribution to  $B_s - \bar{B}_s$  mixing.

#### 4.3 $Z'$ width and perturbativity

The partial width of a  $Z'$  decaying into a Weyl fermion  $f_i$  and and Weyl anti-fermion  $\bar{f}_j$  is

$$\Gamma_{ij} = \frac{C}{24\pi} |g_{ij}|^2 M_{Z'}, \quad (20)$$

where  $g_{ij}$  is the coupling of the  $Z'$  boson to  $f_i \bar{f}_j$  and  $C$  is the number of colour degrees of freedom of the fermions (here, 3 or 1). In the limit that  $m_t/M_{Z'} \rightarrow 0$ , we may approximate all fermions as being massless. Summing over fermion species (it is simplest to do this in the weak eigenbasis), we obtain a total width  $\Gamma$ :

$$\frac{\Gamma}{M_{Z'}} = \frac{13g_{Z'}^2}{8\pi}. \quad (21)$$

To remain in the perturbative régime such that we may trust our perturbative calculations, we should have  $\Gamma/M_{Z'} < 1$ , i.e.  $g_{Z'} < \sqrt{8\pi/13} = 1.4$ . Substituting this into (19) yields an upper bound  $M_{Z'} \leq 29(-0.97/C_9)$  TeV from perturbativity, fits to NCBA and  $B_s - \bar{B}_s$  mixing measurements.

#### 4.4 LHC $Z'$ Searches

The ATLAS experiment has performed various searches in  $pp$  collisions at the LHC for resonant  $Z'$  vector bosons

<sup>4</sup>In the present paper, we quote all single-sided empirical bounds at the 95% confidence level.

decaying into different final states. None of them have found a significant signal to date and so lower limits are placed upon the production cross-sections times branching ratios as a function of the invariant mass of the final state. For example, a  $36.1 \text{ fb}^{-1}$  13 TeV search in  $t\bar{t}$  imposes  $\sigma \times BR(Z' \rightarrow t\bar{t}) < 10$  fb for large  $M_{Z'}$  [65,66]. A di-tau final state search from the 8 TeV run imposes  $\sigma \times BR(Z' \rightarrow \tau^+\tau^-) < 3$  fb for large  $M_{Z'}$  [67]. However, the most constraining channel for the  $(B_3 - L_2)$ eg is from a  $Z' \rightarrow \mu^+\mu^-$  in  $139 \text{ fb}^{-1}$  of 13 TeV  $pp$  collisions [68], where, for  $M_{Z'} = 6$  TeV,  $\sigma \times BR(Z' \rightarrow \mu^+\mu^-) < 0.015$  fb, where  $\sigma$  is the fiducial  $Z'$  production cross-section. We shall therefore use this search to constrain the model<sup>5</sup>. Feynman diagrams of example  $Z'$  production signal processes are shown in Fig. 4.

In this ATLAS di-muon resonance search, each muon is required to have a transverse momentum  $p_T > 30$  GeV, pseudo-rapidity magnitude  $|\eta| < 2.5$  and a di-muon invariant mass  $m_{\mu\mu} > 225$  GeV. ATLAS has already taken efficiencies into account in their published bounds so there is no need to simulate the detector. Upper bounds  $s(M_{Z'}, z)$  on  $\sigma \times BR(Z' \rightarrow \mu^+\mu^-)$  are published for  $z := \Gamma/M_{Z'}$  values from 0 to 0.1 [69]. In Ref. [64], it was shown that a function

$$s(z, M_{Z'}) = s(0, M_{Z'}) \left[ \frac{s(0.1, M_{Z'})}{s(0, M_{Z'})} \right]^{\frac{z}{0.1}} \quad (22)$$

fits the given published bounds well in the given domain  $z \in [0, 0.1]$ . We shall also use (22) to extrapolate slightly outside of this domain, but will delineate regions of parameter space where the bound is extrapolated rather than interpolated.

The  $(B_3 - L_2)$ eg model was encoded into UFO format via `FeynRules` [70,71] for inclusion into an event generator. We calculate the fiducial cross-section  $\sigma(pp \rightarrow Z' \rightarrow \mu^+\mu^-)$  with the `MadGraph_2.6.5` [72] event generator<sup>6</sup> for a centre of mass energy of 13 TeV. We have added the possibility of producing an additional jet along with the  $Z'$  so that the second diagram of Fig. 4 is included in our estimate of the cross-section. We also use five flavour parton distribution functions to re-sum initial state  $b$ -quark logarithms [73] and neglect interference with SM backgrounds. We display an allowed parameter space point ( $M_{Z'} = 3$  TeV,  $g_{Z'} = 0.15$ ) in Table 2. From the table, we can see that the dominant process is  $b\bar{b} \rightarrow Z' \rightarrow \mu^+\mu^-$ , the sub-dominant process is  $(bg \rightarrow Z'b \rightarrow \mu^+\mu^-b + CP \text{ conjugate})$ . The other tree-level processes simulated make a negligible contribution to the cross-section.

<sup>5</sup>The analogous CMS search has yet to be published

<sup>6</sup>The UFO model file can be found in the ancillary information attached to the arXiv preprint version of this paper.

$M_{Z'}$	3 TeV
$g_{Z'}$	0.15
$\sin 2\theta_{sb}$	0.20
$\Gamma$	35 GeV
$s(M_{Z'}, z)$	0.069 fb
$\sigma(pp \rightarrow Z' \rightarrow \mu^+\mu^-) (+j)$	0.033 fb
$BR(Z' \rightarrow \mu^+\mu^-)$	0.46
$BR(Z' \rightarrow t\bar{t})$	0.15
$BR(Z' \rightarrow b\bar{b})$	0.15
$\sigma(b\bar{b} \rightarrow Z' \rightarrow \mu^+\mu^-)$	0.026 fb
$\sigma(gb \rightarrow Z'b \rightarrow \mu^+\mu^-b)$	0.007 fb
$\sigma(s\bar{b} \rightarrow Z' \rightarrow \mu^+\mu^-)$	$6.1 \times 10^{-4}$ fb

**Table 2** Example point in  $(B_3 - L_2)_{eg}$  parameter space that fits the NBCAs (for central  $C_9 = -0.97$ ) and survives all constraints. We show the largest partonic contributions to the cross-section at the bottom of the table. For the last two rows, the  $CP$  conjugated process has been added to the cross-section contribution. ‘(+j)’ refers to the fact that the cross-section includes the addition of another jet in the final state.

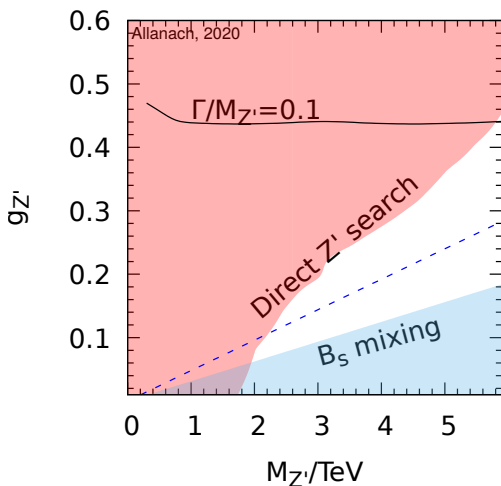


**Fig. 5** Constraints upon  $(B_3 - L_2)_{eg}$ .  $\sin 2\theta_{sb}$  has been set as in (17) such that every point fits the NBCAs. The white region is currently allowed. The red and blue coloured regions show the 95% excluded regions from a 13 TeV  $139 \text{ fb}^{-1}$  ATLAS  $Z' \rightarrow \mu^+\mu^-$  search [68] and from  $B_s - \bar{B}_s$  mixing as in (19), respectively. The latter bound moves from the blue coloured region at lower  $C_9 = -0.65$  to the region below the dashed line for central  $C_9 = -0.97$ . The direct search bound is extrapolated above the solid curve and interpolated between ATLAS data below it, according to (22).

In Fig. 5, we display constraints upon the  $(B_3 - L_2)_{eg}$  parameter space. There is only a small region of parameter space where the ATLAS di-muon resonance search bounds have been extrapolated (slightly): above the solid line. The white region of the figure is allowed by all constraints. We see that  $M_{Z'} > 1.9$  TeV from these. The direct search constraint does not change by eye from the one shown in the figure when one chooses

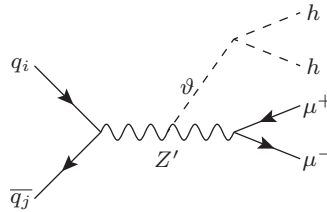


**Fig. 6** Feynman diagram of *flavonstrahlung* process at a hadron collider.  $q_{i,j} \in \{u, c, d, s, b\}$  are such that the combination  $q_i \bar{q}_j$  has zero electric charge.

the central value of  $C_9 = -0.97$  from the NCBA fit or the lower value. We may understand this by the fact that  $\sin 2\theta_{sb}$  is small throughout the vast majority of the plot, whichever value of  $C_9$  is used, in accordance with Fig. 2. The dominant  $Z'$  production amplitude is proportional to the  $Z' \bar{b}b$  coupling, which is proportional to  $g_{Z'} \cos 2\theta_{sb} \approx g_{Z'}$  and so loses the sensitivity<sup>7</sup> that  $\sin 2\theta_{sb}$  has on  $C_9$  through (17). The  $B_s$  mixing bound is however sensitive to a change in  $C_9$  (via its effect on  $g_{sb}$ ) and the bound becomes the dashed line for central  $C_9$ . So: for central  $C_9$ , one concludes that  $M_{Z'} > 2.2$  TeV. For either value of  $C_9$  and throughout the allowed parameter space shown,  $BR(Z' \rightarrow \mu^+\mu^-)$ ,  $BR(Z' \rightarrow \bar{b}b)$  and  $BR(Z' \rightarrow t\bar{t})$  do not change (to the significant figure quoted) from the values in Table 2.

#### 4.5 Flavonstrahlung

In the unbroken  $U(1)_{B_3 - L_2}$  theory,  $\theta$  interacts with the Higgs boson via the Lagrangian density term  $-\lambda_{\theta H} \theta \theta^\dagger H H^\dagger$ . Supposing that the dimensionless coefficient  $\lambda_{\theta H} \neq 0$ , the flavon  $\theta$  will then decay into two physical Higgs bosons  $hh$  with approximately 100% branching ratio. Moreover, the  $\theta$  kinetic term leads to the Lagrangian density term  $g_{Z'}^2 q_\theta^2 Z'_\mu Z'^{\mu} (\theta) \theta$  after spontaneous symmetry breaking. Thus, if a proton-proton collider has sufficient energy and luminosity, it may produce  $Z' \theta$ , leading to the spectacular signature of  $\mu^+\mu^- hh$ , where  $\mu^+\mu^-$  have a resonance at an invariant mass of  $M_{Z'}$  and  $hh$  have one at the flavon mass  $m_\theta$ . This ‘flavonstrahlung’ process is depicted in Fig. 6. Flavonstrahlung would of course not be the first detection of beyond the SM physics in the model:  $Z'$  production followed by decay into  $\mu^+\mu^-$  would most likely be the first, followed perhaps by  $Z' \rightarrow t\bar{t}$  and  $b\bar{b}$ . Flavonstrahlung is suppressed compared to exclusive  $Z'$  production because of its larger final-state phase space and kinematics, and would thus require significantly more luminosity and partonic energy to detect.

<sup>7</sup>(20) and (21) show that  $BR(Z' \rightarrow \mu^+\mu^-)$  has no dependence on  $C_9$  through  $\sin 2\theta_{sb}$  either.

## 5 Discussion

Spontaneously broken  $U(1)_{B_3-L_2}$  has parameter space that is consistent with current direct search limits whilst fitting neutral current  $B$ -anomalies. It simultaneously passes other indirect limits (specifically those from measurements of  $B_s - \overline{B}_s$  mixing).

We have provided a simple broad-brush formulation of the  $U(1)_{B_3-L_2}$  model [42, 44], similar to the one of the Third Family Hypercharge Model (TFHM) [53] and variants [74]. We then presented an example case for phenomenological study, the ‘ $(B_3 - L_2)eg$ ’. The direct  $Z' \rightarrow \mu^+ \mu^-$  search constraints on the  $(B_3 - L_2)eg$  are quite comparable to those on similarly constructed TFHMeg models<sup>8</sup>. In TFHMs though, the Higgs is necessarily charged under the additional  $U(1)$  in order to allow a renormalisable top Yukawa coupling (which seems necessary, given that it is of order 1 and so is inconsistent with a small effective coupling induced by symmetry breaking). This leads to tree-level  $Z - Z'$  mixing and associated strong bounds from inferences of the  $\rho$  parameter [75], and inherited family dependence in  $Z^0$  boson couplings in the TFHMs. The  $U(1)_{B_3-L_2}$  model is not subject to these strong bounds, however, since the SM Higgs doublet remains uncharged under the additional  $U(1)$ .

In §4.5, we have identified a novel flavonstrahlung signal process, where  $pp$  collisions result in  $Z'$  plus flavon production, followed by  $Z'$  decay into  $\mu^+ \mu^-$  and flavon decay into  $hh$ . This process will also be present in other similar NCBA-explaining  $U(1)$  extensions which are broken by a SM singlet, since the flavon field used to break the  $U(1)$  extension will generically have couplings with the SM Higgs doublet. Thus, for example, TFHMs also predict the possibility of flavonstrahlung.

## Acknowledgements

This work has been partially supported by STFC Consolidated HEP grant ST/P000681/1. We thank other members of the Cambridge Pheno Working Group and W. Murray for discussions.

<sup>8</sup>In Refs. [53, 74], the associated production process  $Z'j$  was not included, however.

## Appendix A: Conventions and fermion mixing

Here, we detail the rotation of fermion fields to the mass basis in order to fix our conventions. We write

$$\begin{aligned} \mathbf{u}'_{\mathbf{L}} &= \begin{pmatrix} u'_L \\ c'_L \\ t'_L \end{pmatrix}, & \mathbf{d}'_{\mathbf{L}} &= \begin{pmatrix} d'_L \\ s'_L \\ b'_L \end{pmatrix}, & \boldsymbol{\nu}'_{\mathbf{L}} &= \begin{pmatrix} \nu'_{eL} \\ \nu'_{\mu L} \\ \nu'_{\tau L} \end{pmatrix}, \\ \mathbf{e}'_{\mathbf{L}} &= \begin{pmatrix} e'_L \\ \mu'_L \\ \tau'_L \end{pmatrix}, & \mathbf{u}'_{\mathbf{R}} &= \begin{pmatrix} u'_R \\ c'_R \\ t'_R \end{pmatrix}, & \mathbf{d}'_{\mathbf{R}} &= \begin{pmatrix} d'_R \\ s'_R \\ b'_R \end{pmatrix}, \\ \mathbf{e}'_{\mathbf{R}} &= \begin{pmatrix} e'_R \\ \mu'_R \\ \tau'_R \end{pmatrix}, & \boldsymbol{\nu}'_{\mathbf{R}} &= \begin{pmatrix} \nu'_{eR} \\ \nu'_{\mu R} \\ \nu'_{\tau R} \end{pmatrix}, \end{aligned} \quad (\text{A.1})$$

along with the SM fermionic electroweak doublets

$$\mathbf{Q}'_{\mathbf{L}i} = \begin{pmatrix} \mathbf{u}'_{\mathbf{L}i} \\ \mathbf{d}'_{\mathbf{L}i} \end{pmatrix}, \quad \mathbf{L}'_{\mathbf{L}i} = \begin{pmatrix} \boldsymbol{\nu}'_{\mathbf{L}i} \\ \mathbf{e}'_{\mathbf{L}i} \end{pmatrix}. \quad (\text{A.2})$$

The fermions acquire their masses through the terms

$$-\mathcal{L}_Y = \overline{\mathbf{Q}'_{\mathbf{L}}} Y_u \tilde{H} \mathbf{u}'_{\mathbf{R}} + \overline{\mathbf{Q}'_{\mathbf{L}}} Y_d H \mathbf{d}'_{\mathbf{R}} + \overline{\mathbf{L}'_{\mathbf{L}}} Y_e H \mathbf{e}'_{\mathbf{R}} + \overline{\mathbf{L}'_{\mathbf{L}}} Y_\nu \tilde{H} \boldsymbol{\nu}'_{\mathbf{R}} + H.c. + \frac{1}{2} \overline{\boldsymbol{\nu}'_{\mathbf{R}}} M \boldsymbol{\nu}'_{\mathbf{R}}, \quad (\text{A.3})$$

where  $Y_u$ ,  $Y_d$  and  $Y_e$  are dimensionless complex coupling constants, each written as a 3 by 3 matrix in family space. The matrix  $M$  is a 3 by 3 complex symmetric matrix of mass dimension 1,  $^c$  denotes the charge conjugate of a field and  $\tilde{H} = (H^{0*}, -H^-)^T$ . After electroweak symmetry breaking and the  $W^\pm$  boson eating the electrically charged components of the Higgs doublet, we may write  $H = (0, (v+h)/\sqrt{2})$ , where  $v$  is the Higgs vacuum expectation value,  $h$  is the physical Higgs boson field and (A.3) includes the fermion mass terms

$$\begin{aligned} -\mathcal{L}_Y &= \overline{\mathbf{u}'_{\mathbf{L}}} V_{uL} V_{uL}^\dagger m_u V_{uR} V_{uR}^\dagger \mathbf{u}'_{\mathbf{R}} + \\ &\overline{\mathbf{d}'_{\mathbf{L}}} V_{dL} V_{dL}^\dagger m_d V_{dR} V_{dR}^\dagger \mathbf{d}'_{\mathbf{R}} + \\ &\overline{\mathbf{e}'_{\mathbf{L}}} V_{eL} V_{eL}^\dagger m_e V_{eR} V_{eR}^\dagger \mathbf{e}'_{\mathbf{R}} + \\ &\frac{1}{2} (\overline{\boldsymbol{\nu}'_{\mathbf{L}}} \overline{\boldsymbol{\nu}'_{\mathbf{R}}}) M_\nu \begin{pmatrix} \boldsymbol{\nu}'_{\mathbf{L}} \\ \boldsymbol{\nu}'_{\mathbf{R}} \end{pmatrix} + H.c. \\ &+ \dots, \end{aligned} \quad (\text{A.4})$$

where

$$M_\nu = \begin{pmatrix} 0 & m_{\nu D} \\ m_{\nu D}^T & M \end{pmatrix}, \quad (\text{A.5})$$

$V_{I_L}$  and  $V_{I_R}$  are 3 by 3 unitary mixing matrices for each species  $I$ ,  $m_u := vY_u/\sqrt{2}$ ,  $m_d := vY_d/\sqrt{2}$ ,  $m_e := vY_e/\sqrt{2}$  and  $m_{\nu D} := vY_\nu/\sqrt{2}$ . The final explicit term in (A.4) incorporates the see-saw mechanism via a 6 by 6 complex symmetric mass matrix. Since the elements in  $m_{\nu D}$  are much less than those in  $M$ , one performs a rotation to obtain a 3 by 3 complex symmetric mass

matrix for the *light* neutrinos. To a good approximation, these coincide with the left-handed weak eigenstates  $\nu'_L$ , whereas three heavy neutrinos approximately correspond to the right-handed weak eigenstates  $\nu'_R$ . The neutrino mass term of (A.4) becomes, to a good approximation,

$$-\mathcal{L}_\nu = \frac{1}{2} \overline{\nu'_L} m_\nu \nu'_L + \frac{1}{2} \overline{\nu'_R} M \nu'_R + H.c., \quad (\text{A.6})$$

where  $m_\nu := m_{\nu_D}^T M^{-1} m_{\nu_D}$  is a complex symmetric 3 by 3 matrix.

Choosing  $V_{IL}^\dagger m_I V_{IR}$  to be diagonal, real and positive for  $I \in \{u, d, e\}$ , and  $V_{\nu L}^T m_\nu V_{\nu L}$  to be diagonal, real and positive (all in increasing order of mass from the top left toward the bottom right of the matrix), we can identify the *non-primed mass* eigenstates

$$\begin{aligned} \mathbf{u}_R &:= V_{uR}^\dagger \mathbf{u}'_R, & \mathbf{u}_L &:= V_{uL}^\dagger \mathbf{u}'_L, & \mathbf{d}_R &:= V_{dR}^\dagger \mathbf{d}'_R, \\ \mathbf{d}_L &:= V_{dL}^\dagger \mathbf{d}'_L, & \mathbf{e}_R &:= V_{eR}^\dagger \mathbf{e}'_R, & \mathbf{e}_L &:= V_{eL}^\dagger \mathbf{e}'_L. \\ \nu_L &:= V_{\nu L}^\dagger \nu'_L. \end{aligned} \quad (\text{A.7})$$

We may then find the CKM matrix  $V$  and the Pontecorvo-Maki-Nakagawa-Sakata (PMNS) matrix  $U$  in terms of the fermionic mixing matrices:

$$V = V_{uL}^\dagger V_{dL}, \quad U = V_{\nu L}^\dagger V_{eL}. \quad (\text{A.8})$$

## References

1. R. Aaij, et al., JHEP **08**, 055 (2017). DOI 10.1007/JHEP08(2017)055
2. R. Aaij, et al., Phys. Rev. Lett. **122**(19), 191801 (2019). DOI 10.1103/PhysRevLett.122.191801
3. M. Aaboud, et al., JHEP **04**, 098 (2019). DOI 10.1007/JHEP04(2019)098
4. S. Chatrchyan, et al., Phys. Rev. Lett. **111**, 101804 (2013). DOI 10.1103/PhysRevLett.111.101804
5. V. Khachatryan, et al., Nature **522**, 68 (2015). DOI 10.1038/nature14474
6. R. Aaij, et al., Phys. Rev. Lett. **118**(19), 191801 (2017). DOI 10.1103/PhysRevLett.118.191801
7. R. Aaij, et al., Phys. Rev. Lett. **111**, 191801 (2013). DOI 10.1103/PhysRevLett.111.191801
8. R. Aaij, et al., JHEP **02**, 104 (2016). DOI 10.1007/JHEP02(2016)104
9. M. Aaboud, et al., JHEP **10**, 047 (2018). DOI 10.1007/JHEP10(2018)047
10. A.M. Sirunyan, et al., Phys. Lett. B **781**, 517 (2018). DOI 10.1016/j.physletb.2018.04.030
11. V. Khachatryan, et al., Phys. Lett. **B753**, 424 (2016). DOI 10.1016/j.physletb.2015.12.020
12. C. Bobeth, M. Chruszcz, D. van Dyk, J. Virto, Eur. Phys. J. **C78**(6), 451 (2018). DOI 10.1140/epjc/s10052-018-5918-6
13. P.A. Zyla, et al., PTEP **2020**(8), 083C01 (2020). DOI 10.1093/ptep/ptaa104
14. M. Alguer, B. Capdevila, A. Crivellin, S. Descotes-Genon, P. Masjuan, J. Matias, M. Novoa Brunet, J. Virto, Eur. Phys. J. **C79**(8), 714 (2019). DOI 10.1140/epjc/s10052-019-7216-3, 10.1140/epjc/s10052-020-8018-3. [Addendum: Eur. Phys. J. **C80**, no. 6, 511 (2020)]
15. A.K. Alok, A. Dighe, S. Gangal, D. Kumar, JHEP **06**, 089 (2019). DOI 10.1007/JHEP06(2019)089
16. M. Ciuchini, A.M. Coutinho, M. Fedele, E. Franco, A. Paul, L. Silvestrini, M. Valli, Eur. Phys. J. **C79**(8), 719 (2019). DOI 10.1140/epjc/s10052-019-7210-9
17. J. Aebischer, W. Altmannshofer, D. Guadagnoli, M. Reboud, P. Stangl, D.M. Straub, Eur. Phys. J. **C80**(3), 252 (2020). DOI 10.1140/epjc/s10052-020-7817-x
18. K. Kowalska, D. Kumar, E.M. Sessolo, Eur. Phys. J. **C79**(10), 840 (2019). DOI 10.1140/epjc/s10052-019-7330-2
19. A. Arbey, T. Hurth, F. Mahmoudi, D.M. Santos, S. Neshatpour, Phys. Rev. **D100**(1), 015045 (2019). DOI 10.1103/PhysRevD.100.015045
20. J. Ellis, M. Fairbairn, P. Tunney, Eur. Phys. J. **C78**(3), 238 (2018). DOI 10.1140/epjc/s10052-018-5725-0
21. B.C. Allanach, J. Davighi, S. Melville, JHEP **02**, 082 (2019). DOI 10.1007/JHEP08(2019)064, 10.1007/JHEP02(2019)082. [erratum: JHEP08,064(2019)]
22. R. Gauld, F. Goertz, U. Haisch, Phys. Rev. **D89**, 015005 (2014). DOI 10.1103/PhysRevD.89.015005
23. A.J. Buras, F. De Fazio, J. Girrbach, JHEP **02**, 112 (2014). DOI 10.1007/JHEP02(2014)112
24. A.J. Buras, J. Girrbach, JHEP **12**, 009 (2013). DOI 10.1007/JHEP12(2013)009
25. W. Altmannshofer, S. Gori, M. Pospelov, I. Yavin, Phys. Rev. **D89**, 095033 (2014). DOI 10.1103/PhysRevD.89.095033
26. A.J. Buras, F. De Fazio, J. Girrbach-Noe, JHEP **08**, 039 (2014). DOI 10.1007/JHEP08(2014)039
27. A. Crivellin, G. D'Ambrosio, J. Heeck, Phys. Rev. Lett. **114**, 151801 (2015). DOI 10.1103/PhysRevLett.114.151801
28. A. Crivellin, G. D'Ambrosio, J. Heeck, Phys. Rev. **D91**(7), 075006 (2015). DOI 10.1103/PhysRevD.91.075006
29. D. Aristizabal Sierra, F. Staub, A. Vicente, Phys. Rev. **D92**(1), 015001 (2015). DOI 10.1103/PhysRevD.92.015001
30. A. Crivellin, L. Hofer, J. Matias, U. Nierste, S. Pokorski, J. Rosiek, Phys. Rev. **D92**(5), 054013 (2015). DOI 10.1103/PhysRevD.92.054013
31. A. Celis, J. Fuentes-Martin, M. Jung, H. Serodio, Phys. Rev. **D92**(1), 015007 (2015). DOI 10.1103/PhysRevD.92.015007
32. A. Greljo, G. Isidori, D. Marzocca, JHEP **07**, 142 (2015). DOI 10.1007/JHEP07(2015)142
33. W. Altmannshofer, I. Yavin, Phys. Rev. **D92**(7), 075022 (2015). DOI 10.1103/PhysRevD.92.075022
34. B. Allanach, F.S. Queiroz, A. Strumia, S. Sun, Phys. Rev. **D93**(5), 055045 (2016). DOI 10.1103/PhysRevD.93.055045, 10.1103/PhysRevD.95.119902. [Erratum: Phys. Rev. **D95**, no. 11, 119902(2017)]
35. A. Falkowski, M. Nardecchia, R. Ziegler, JHEP **11**, 173 (2015). DOI 10.1007/JHEP11(2015)173
36. C.W. Chiang, X.G. He, G. Valencia, Phys. Rev. **D93**(7), 074003 (2016). DOI 10.1103/PhysRevD.93.074003
37. D. Beirevi, O. Sumensari, R. Zukanovich Funchal, Eur. Phys. J. **C76**(3), 134 (2016). DOI 10.1140/epjc/s10052-016-3985-0
38. S.M. Boucenna, A. Celis, J. Fuentes-Martin, A. Vicente, J. Virto, Phys. Lett. **B760**, 214 (2016). DOI 10.1016/j.physletb.2016.06.067
39. S.M. Boucenna, A. Celis, J. Fuentes-Martin, A. Vicente, J. Virto, JHEP **12**, 059 (2016). DOI 10.1007/JHEP12(2016)059

40. P. Ko, Y. Omura, Y. Shigekami, C. Yu, Phys. Rev. **D95**(11), 115040 (2017). DOI 10.1103/PhysRevD.95.115040
41. R. Alonso, P. Cox, C. Han, T.T. Yanagida, Phys. Rev. **D96**(7), 071701 (2017). DOI 10.1103/PhysRevD.96.071701
42. R. Alonso, P. Cox, C. Han, T.T. Yanagida, Phys. Lett. **B774**, 643 (2017). DOI 10.1016/j.physletb.2017.10.027
43. Y. Tang, Y.L. Wu, Chinese Physics C **42**(3), 033104 (2018). URL <http://stacks.iop.org/1674-1137/42/i=3/a=033104>
44. C. Bonilla, T. Modak, R. Srivastava, J.W.F. Valle, Phys. Rev. **D98**(9), 095002 (2018). DOI 10.1103/PhysRevD.98.095002
45. D. Bhatia, S. Chakraborty, A. Dighe, JHEP **03**, 117 (2017). DOI 10.1007/JHEP03(2017)117
46. C.H. Chen, T. Nomura, Physics Letters B **777**, 420 (2018). DOI <https://doi.org/10.1016/j.physletb.2017.12.062>. URL <http://www.sciencedirect.com/science/article/pii/S0370269318300029>
47. G. Faisel, J. Tandean, JHEP **02**, 074 (2018). DOI 10.1007/JHEP02(2018)074
48. K. Fuyuto, H.L. Li, J.H. Yu, Phys. Rev. D **97**, 115003 (2018). DOI 10.1103/PhysRevD.97.115003. URL <https://link.aps.org/doi/10.1103/PhysRevD.97.115003>
49. L. Bian, H.M. Lee, C.B. Park, Eur. Phys. J. C **78**(4), 306 (2018). DOI 10.1140/epjc/s10052-018-5777-1
50. M. Abdullah, M. Dalchenko, B. Dutta, R. Eusebi, P. Huang, T. Kamon, D. Rathjens, A. Thompson, Phys. Rev. D **97**, 075035 (2018). DOI 10.1103/PhysRevD.97.075035. URL <https://link.aps.org/doi/10.1103/PhysRevD.97.075035>
51. S.F. King, JHEP **09**, 069 (2018). DOI 10.1007/JHEP09(2018)069
52. G.H. Duan, X. Fan, M. Frank, C. Han, J.M. Yang, Phys. Lett. **B789**, 54 (2019). DOI 10.1016/j.physletb.2018.12.005
53. B.C. Allanach, J. Davighi, JHEP **12**, 075 (2018). DOI 10.1007/JHEP12(2018)075
54. B.C. Allanach, T. Corbett, M.J. Dolan, T. You, JHEP **03**, 137 (2019). DOI 10.1007/JHEP03(2019)137
55. Z. Kang, Y. Shigekami, JHEP **11**, 049 (2019). DOI 10.1007/JHEP11(2019)049
56. J. Davighi, M. Kirk, M. Nardecchia, (2020)
57. A. Crivellin, J. Fuentes-Martin, A. Greljo, G. Isidori, Phys. Lett. **B766**, 77 (2017). DOI 10.1016/j.physletb.2016.12.057
58. J.F. Kamenik, Y. Soreq, J. Zupan, Phys. Rev. **D97**(3), 035002 (2018). DOI 10.1103/PhysRevD.97.035002
59. J.E. Camargo-Molina, A. Celis, D.A. Faroughy, Phys. Lett. **B784**, 284 (2018). DOI 10.1016/j.physletb.2018.07.051
60. F. Englert, R. Brout, Phys. Rev. Lett. **13**, 321 (1964). DOI 10.1103/PhysRevLett.13.321. URL <https://link.aps.org/doi/10.1103/PhysRevLett.13.321>
61. P.W. Higgs, Phys. Rev. Lett. **13**, 508 (1964). DOI 10.1103/PhysRevLett.13.508. URL <https://link.aps.org/doi/10.1103/PhysRevLett.13.508>
62. Y. Amhis, et al., Eur. Phys. J. C **77**(12), 895 (2017). DOI 10.1140/epjc/s10052-017-5058-4
63. D. King, A. Lenz, T. Rauh, JHEP **05**, 034 (2019). DOI 10.1007/JHEP05(2019)034
64. B.C. Allanach, J.M. Butterworth, T. Corbett, JHEP **08**, 106 (2019). DOI 10.1007/JHEP08(2019)106
65. M. Aaboud, et al., Eur. Phys. J. C **78**(7), 565 (2018). DOI 10.1140/epjc/s10052-018-5995-6
66. M. Aaboud, et al., Phys. Rev. **D99**(9), 092004 (2019). DOI 10.1103/PhysRevD.99.092004
67. G. Aad, et al., JHEP **07**, 157 (2015). DOI 10.1007/JHEP07(2015)157
68. G. Aad, et al., Phys. Lett. **B796**, 68 (2019). DOI 10.1016/j.physletb.2019.07.016
69. G. Aad, et al. Search for high-mass dilepton resonances using 139 fb<sup>-1</sup> of pp collision data collected at  $\sqrt{s} = 13$  TeV with the ATLAS detector (2019). DOI <https://doi.org/10.17182/hepdata.88425>. <https://www.hepdata.net/record/88425>
70. C. Degrande, C. Duhr, B. Fuks, D. Grellscheid, O. Mattelaer, T. Reiter, Comput. Phys. Commun. **183**, 1201 (2012). DOI 10.1016/j.cpc.2012.01.022
71. A. Alloul, N.D. Christensen, C. Degrande, C. Duhr, B. Fuks, Comput. Phys. Commun. **185**, 2250 (2014). DOI 10.1016/j.cpc.2014.04.012
72. J. Alwall, R. Frederix, S. Frixione, V. Hirschi, F. Maltoni, O. Mattelaer, H.S. Shao, T. Stelzer, P. Torrielli, M. Zaro, JHEP **07**, 079 (2014). DOI 10.1007/JHEP07(2014)079
73. M. Lim, F. Maltoni, G. Ridolfi, M. Ubiali, JHEP **09**, 132 (2016). DOI 10.1007/JHEP09(2016)132
74. B. Allanach, J. Davighi, Eur. Phys. J. C **79**(11), 908 (2019). DOI 10.1140/epjc/s10052-019-7414-z
75. J. Davighi, Topological effects in particle physics phenomenology. Ph.D. thesis, Cambridge U. (main) (2020). DOI 10.17863/CAM.47560